Power Plant Controller Compliance and Validation via Hardware-in-the-Loop

Seyedehniloofar Kamalhosseini[1,2], Timo Wagner[1], Eckart Brackenhammer[2],
Ilya Burlakin[1], Gert Mehlmann[1], Matthias Luther[1]
[1]*Institute of Electrical Energy Systems*
Friedrich-Alexander-Universität Erlangen-Nürnberg
[2]*Smart Infrastructure, Siemens AG*
Erlangen, Germany
niloofar.kamalhosseini@fau.de
seyedehniloofar.kamalhosseini@siemens.com

***Abstract*—This paper presents a comprehensive validation of a Power Plant Controller (PPC) by benchmarking its Root Mean Square (RMS) simulation model against the operational behavior of the physical hardware. The validation is performed using Controller Hardware-in-the-Loop (CHiL) testing with a Real-Time Digital Simulator (RTDS®), enabling high-fidelity comparisons under realistic grid conditions. All testing procedures are conducted in accordance with the German grid code requirements. The dynamic performance of the PPC model is evaluated through a series of extensive test scenarios, including responses to voltage and frequency deviations, active and reactive power setpoint changes, and power factor regulation. The results confirm the accuracy and reliability of the RMS simulation model in replicating the behavior of the actual hardware, thereby enabling its use in grid code compliance studies.**

***Index Terms*—Controller Hardware-in-the-Loop, Grid Code Compliance, Power Plant Controller, Real-Time Digital Simulator, Renewable Power Plants**

I. Introduction

The increasing integration of inverter-based resources (IBRs) has increased the complexity of grid code compliance and introduced new challenges in power system design and validation. The dynamic behavior of IBRs at the point of common coupling (PCC) must be evaluated according to national grid code requirements, often necessitating project-specific user defined models (UDMs) due to diverse regulations and multi-vendor plant configurations. Accurate model development therefore requires detailed knowledge of plant-level control strategies and collaboration with manufacturers and system operators [1].

In large-scale renewable power plants (RPPs), grid compliance is typically achieved through a Power Plant Controller (PPC), which coordinates inverter operation and regulates aggregated active and reactive power at the PCC [2]. As a central supervisory component, the PPC must be accurately represented in simulation studies and modeled consistently with its hardware implementation [3].

PPC deployment typically begins with the development of a simulation model reflecting controller functionality, followed by project-specific grid compliance studies and on-site commissioning tests to verify operational performance and reduce implementation risks [4], [5].

Prior to commissioning, preliminary simulation studies are required. In this context, Root Mean Square (RMS) simulation remains a primary tool for grid compliance and stability assessment due to its computational efficiency and suitability for balanced and quasi-steady-state system analysis [6]. Consequently, Transmission System Operators (TSOs) rely on validated RMS models for routine planning, operational studies, and compliance verification [7]. However, numerical approximations and implementation details, such as PI control algorithms, deadbands, anti-windup mechanisms, and signal filtering can introduce discrepancies between simulated and physical PPC behavior. Therefore, validating simulation models against physical controllers using Controller Hardware-in-the-Loop (CHiL) testing is essential for reliable compliance assessment. CHiL testing enables performance evaluation under realistic operating conditions by integrating the actual controller hardware into a real-time simulation environment [8]. Prior studies [9], [10], [11] have predominantly focused on hardware-level validation rather than systematic benchmarking of RMS simulation models against physical PPC implementations under grid-code-driven test scenarios.

This paper presents a CHiL-based validation of an RMS PPC model against a commercially deployed controller implemented on a Siemens SICAM A8000 RTU platform, in accordance with German grid code requirements [12], [13], [14]. Although demonstrated using a PV-based plant, the proposed validation framework is applicable to a wide range of inverter-based technologies operating under PPC supervision. The RMS model is developed in DIgSILENT PowerFactory, while an RTDS® platform provides realistic grid conditions for synchronized hardware model benchmarking. The main contributions of this work are: (a) a CHiL-based benchmarking methodology for validating RMS PPC models against physical hardware, (b) quantitative comparison of plant dynamic responses under grid-code-driven scenarios, and (c) practical modeling and validation guidelines for plant-level controllers.

The structure of this paper is as follows: Section II describes the CHiL and simulation setup, Section III presents PPC functionalities, Section IV discusses validation results, and Section V concludes the paper.

979-8-3315-8138-1

II. Test Setup for CHiL and Simulation Environment

This section describes the configurations used for CHiL testing and offline RMS simulations. The RTDS platform enables real-time interaction between the PPC hardware and the simulated grid, while the RMS environment supports offline compliance analysis and model benchmarking.

A. CHiL Test Setup

The network model is implemented in the RTDS RSCAD environment. The test grid, depicted in Fig. 1, includes several essential components. The high-voltage grid is modeled using a Thevenin equivalent set at $220\,\mathrm{kV}$, $250\,\mathrm{MVA}$, and $50\,\mathrm{Hz}$, with an R/X ratio of 0.1. Electrical quantities at PCC are measured via current and voltage transformers. Voltage levels are stepped down through a series of transformers: From high-voltage ($220\,\mathrm{kV}$) to medium-voltage ($33\,\mathrm{kV}$), and subsequently to low-voltage ($0.69\,\mathrm{kV}$). The two aggregated PV units are modeled as average models with three controlled AC voltage sources. The DC side is not represented. Converter control is implemented in the rotating dq-coordinate system following [15]. Reference currents for the d- and q-axis PI controllers are computed from the desired active and reactive power setpoints as

$$i_{d,\mathrm{ref}} = \frac{2}{3}\frac{P_{\mathrm{set}}\ u_d + Q_{\mathrm{set}}\ u_q}{u_d^2 + u_q^2}, \tag{1}$$

$$i_{q,\mathrm{ref}} = \frac{2}{3}\frac{P_{\mathrm{set}}\ u_d - Q_{\mathrm{set}}\ u_q}{u_d^2 + u_q^2}, \tag{2}$$

where u_d and u_q are the measured d- and q-axis voltages, respectively. The power setpoints are transmitted from the controller to the simulation model. This RMS-level representation is sufficient for plant-level PPC benchmarking, since EMT switching transients have negligible impact on aggregated controller responses. Each PV system is rated at $4.5\,\mathrm{MW}$, resulting in a total nominal plant capacity of $9\,\mathrm{MW}$.

The network model in RSCAD interfaces with the PPC, serving as the Device under Test (DuT), through Modbus/TCP. The simulated three-phase voltages and current signals at the PCC are measured with transducers. These signals are scaled within RSCAD and transmitted as physical analog outputs via the Generic Time Averaged Output (GTAO) card in the RTDS hardware rack to a measurement amplifier (Omicron CMS356), which is connected to the measurement unit of the PPC (SICAM T). The analogue measuring card of the PPC is used to capture control values of active and reactive power directly. Measurement data and evaluated parameters are transmitted as digital packages to the PPC. The PPC processes these inputs and computes corresponding control commands, which are sent to the simulated PV units within the RTDS environment, thereby closing the control loop between the simulated grid and the physical controller.

Furthermore, RTDS enables dynamic adjustment of grid voltage and frequency during runtime, which is utilized in various test scenarios discussed in Section IV.

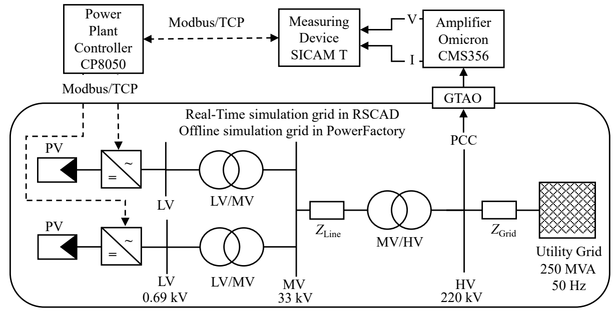

Fig. 1. CHiL test configuration.

B. Offline RMS Simulation

Offline simulations are conducted in DIgSILENT PowerFactory 2023 SP3 (x64), where the SICAM PPC is implemented as a UDM. The same grid configuration and parameters as shown in Fig. 1 are reproduced to enable direct comparison between RMS simulations and CHiL measurements. The interconnection between the PPC and the inverter is illustrated in Fig. 2. The PPC, as a high-level supervisory controller, receives various signals from the measurement devices and includes multiple active and reactive power control modes, which are detailed in Section III.

Based on the applicable grid code requirements, the PPC determines the corresponding power setpoints and communicates them to the inverters operating under primary control. This coordination is performed through a dispatching function, which evaluates the operational status of each inverter and allocates the respective active and reactive power setpoints accordingly.

III. PPC functionalities

The core functionalities of the implemented UDM PPC comprise multiple active and reactive power control modes, as schematically illustrated in Fig. 3.

A. Active power control loops

1) Maximum power point tracking (MPPT): In this default operating mode, the PPC commands all inverters to inject the maximum available active power.

2) Active power limit control: This mode focuses on minimizing active power deviations at the PCC. The active power setpoint is defined by the operator, and the active power reference (P_{ref}) is initialized to this steady-state value. Any setpoint adjustment will be applied using a predefined ramp rate.

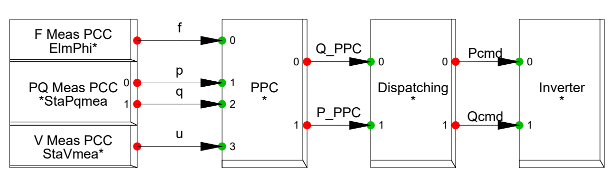

Fig. 2. PPC composite frame in DIgSILENT Powerfactory.

979-8-3315-8138-1

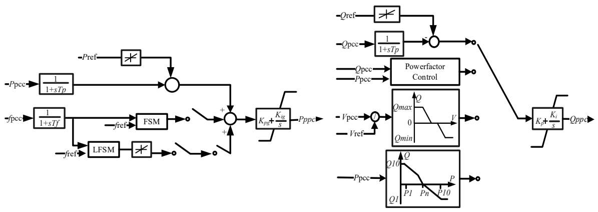

(a) (b)

Fig. 3. Control loops of the implemented UDM PPC: a) Active power, b) Reactive power.

3) Active power feed-in as a function of the grid frequency: This path becomes active when the grid frequency exceeds a predefined deadband. In the Network Code Requirements for Generators (NC RfG), this functionality is referred to as Limited Frequency Sensitive Mode (LFSM) [16]. The change in active power ΔP is calculated using

$$\Delta P = \frac{f_\mathrm{n} + \mathrm{deadband} - f_\mathrm{act}}{f_\mathrm{n}} \frac{P_\mathrm{n}}{\mathrm{Droop}}, \tag{3}$$

where f_n and f_act denote the nominal and actual frequency, respectively. P_n can represent either the steady-state active power P_act at the PCC or the installed active power capacity P_nom in operation [12].

4) Frequency Sensitive Mode (FSM): According to the German grid code for extra-high-voltage [14] and high-voltage [13] connections, power plants must be technically capable of providing primary control. The FSM enables frequency-dependent active power adjustment during normal grid operation. The droop is defined as [17]

$$\mathrm{Droop}\ [\%] = 100\ \frac{|\Delta f|\ P_\mathrm{n}}{f_\mathrm{n}\ \Delta P}, \tag{4}$$

where Δf and ΔP denote frequency deviation and change of the active power output of the plant, respectively. Furthermore, a frequency insensitivity threshold can be configured to avoid unnecessary regulation for minor deviations [17]. Fig. 4(a) depicts the FSM response in case of no deadband and zero insensitivity.

B. Reactive power control loops

A reactive power setpoint can either be manually defined by the operator or automatically calculated based on a characteristic curve corresponding to the selected control mode. The PPC considers inverter P-Q capabilities and the saturation limits of the RPP to optimize reactive power support within operational constraints.

1) Reactive power control: This mode represents the most fundamental approach to reactive power regulation. A constant reactive power setpoint is defined by the operator. Subsequently, the PPC adjusts the output of the plant to achieve this value at the PCC. The reactive power reference (Q_ref) is initialized to this steady-state value, and any setpoint adjustment will be applied using a predefined ramp rate.

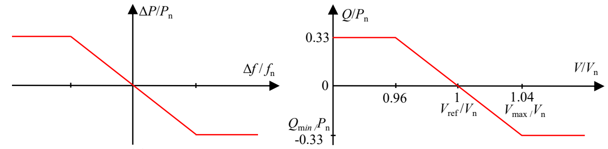

(a) (b)

Fig. 4. PPC characteristics: a) Droop characteristic in FSM [13], b) $Q(V)$ characteristic [12].

2) Power factor control: The PPC maintains a specified power factor at the PCC. The default setpoint is typically $\cos\varphi = 1$. Based on the desired power factor, the PPC adjusts the reactive power output of inverters accordingly.

3) Voltage dependent reactive power control, $Q(V)$: This mode is an advanced and automated voltage control used to support grid stability. The PPC adjusts the reactive power output of the RPP in response to grid voltage variations according to a configurable droop characteristic curve, as shown in Fig. 4(b). The reference voltage corresponding to zero reactive power exchange ($V_\mathrm{ref}/V_\mathrm{n}$), along with the predefined pair ($V_\mathrm{max}/V_\mathrm{n}$, $Q_\mathrm{min}/P_\mathrm{n}$), is specified by the system operator. These parameters determine the slope of the characteristic. Additionally, a deadband can be configured. Within the defined deadband, no reactive power exchange is established. However, when the voltage magnitude deviates beyond this range, the PPC responds dynamically by injecting reactive power during undervoltage conditions and absorbing reactive power during overvoltage conditions.

4) Reactive power dependent active power control: This mode enables automated reactive power generation based on the current active power output of the plant. A predefined $Q(P)$ characteristic curve, typically set in accordance with regional grid code requirements, maps specific active power levels to corresponding reactive power targets. The PPC dynamically adjusts reactive power to follow this curve.

IV. Simulation Results

The PPC is validated across all control modes, provided in Section III. Validation tests follow the FGW Technical Guideline [18], which outlines standardized procedures for assessing grid code compliance of generation units. Equivalent test scenarios are defined in the RMS simulation to benchmark the PPC against its physical hardware. Selected results from simulation cases are presented alongside corresponding CHiL measurements.

The CHiL measurement signals are processed using a discrete Fourier-based fundamental extraction, followed by symmetrical component decomposition to obtain positive-sequence quantities, in accordance with [18], prior to comparison with RMS simulation results.

Extended simulation times are required to capture slow plant-level control dynamics, accommodate multiple test scenarios sequentially, comply with slow ramp-rate requirements, and satisfy German grid code specifications for model validation procedures.

979-8-3315-8138-1

CHiL testing also captures typical feedback and communication delays inherent in commercial implementations. Total system delay arises from protocol polling, signal processing, and measurement-unit latencies. These delays vary over time. Thus, no single fixed value applies. Average delay times are determined for each test case and can be incorporated into simulations as needed. For grid voltage or frequency variation scenarios, a playback method is used: The RTDS directly adapts the grid conditions during CHiL tests, while analogous changes are applied to the Thevenin equivalent external grid in RMS simulations.

The accuracy of the RMS simulation model is evaluated using predefined tolerance bands for both steady-state and dynamic responses. According to [19], permissible deviation for active and reactive power is $0.05\,\mathrm{pu}$ at the stationary target value and up to $0.15\,\mathrm{pu}$ during dynamic transitions. All evaluated parameters remain within these specified tolerance limits in the subsequent simulation results.

A. Power factor control

To test this mode, the active power of the plant is set to $50\,\%$ of its installed capacity and the reactive power is maintained at $Q = 0\ \mathrm{Mvar}$, resulting in a steady-state power factor of $\cos\varphi = 1$. Subsequently, step changes are applied to the power factor reference, $\cos(\varphi)_{\mathrm{ref}}$. In the CHiL test $\cos\varphi$ is adjusted via the Human-Machine Interface of the PPC. In the RMS simulation $\cos(\varphi)_{\mathrm{ref}}$ of the PPC is changed using event definitions. The sequence of applied step changes is summarized in Table I(a), and the corresponding results are illustrated in Fig. 5. As expected, the reactive power of the plant is adjusted to achieve the target power factor at the PCC, while active power remains constant.

B. Voltage dependent reactive power control

Voltage dependency tests are performed using two methods: First, by modifying the grid voltage magnitude V_{grid} via playback method. Second, by adjusting the PPC voltage reference. The results obtained using playback method are presented in Fig. 6, while the corresponding voltage step changes are summarized in Table I(b). For this test, the $Q(V)$ curve was set according to Fig. 4(b), ensuring that at a voltage of $1.04\,\mathrm{pu}$ the reactive power at the PCC attains $-0.33\,\mathrm{pu}$.

C. Active power dependent reactive power control

The $Q(P)$ control function is tested in accordance with the specifications outlined in [12]. To evaluate its performance, step changes are applied to the active power setpoint, as detailed in Table I(c). Transitions in active power are implemented using a ramp function with a defined gradient of $0.66\,\%/\mathrm{s}$ of the installed active power capacity. Each setpoint is maintained for at least 2 minutes, allowing 1 minute for transient settling before calculating 1 minute averaged values of reactive power and the corresponding setpoint.

TABLE I
APPLIED STEP CHANGES DURING TESTS

(a)		(b)		(c)		(d)		(e)	
time (s)	$\cos(\varphi)_{\mathrm{ref}}$	time (s)	V_{grid} (pu)	time (s)	P_{ref} (pu)	time (s)	f_{grid} (Hz)	time (s)	f_{grid} (Hz)
39	-0.95	109	1.09	132	0.75	430	49.7	68	50.1
122	0.95	195	0.915	338	0.6	510	47.6	997	50
208	1.00	282	1.00	520	0.55	582	48.6	1084	49.9
				714	0.5	651	49.7	20163	50
				885	0.0				

D. Active power feed-in as a function of frequency

For this test, the PPC operates with the activated LFSM. The grid frequency is varied using the playback method, covering both over- and under-frequency scenarios. The droop, used in (3), is set to $5\,\%$ and the installed active power capacity is considered for P_{n}. The frequency profile for the under-frequency scenario is provided in Table I(d). Since the objective of the test is to analyze the dynamic response of the PPC, it is conducted under the assumption that sufficient active power reserve is available, for example via curtailment. The corresponding results are shown in Fig. 8.

E. Primary control power provision

The FSM functionality is evaluated following the configurations outlined in [13]. A droop setting of $4\,\%$ is applied. The playback method is employed to vary the grid frequency. In response, the PPC adjusts its active power output according to the configured characteristic curve, thereby providing primary frequency control as required. The applied frequency changes are summarized in Table I(e), and the corresponding results are illustrated in Fig. 9.

V. CONCLUSION

The dynamic behavior of the PPC is validated in accordance with the German grid code using CHiL testing, and its RMS model is benchmarked against the corresponding physical hardware. The RMS model is implemented in DIgSILENT PowerFactory, while the physical controller is interfaced with an RTDS platform as the DuT for CHiL tests. A high degree of agreement is observed between measured hardware responses and RMS simulation results across all evaluated scenarios. The responses consistently remained within prescribed tolerance bands, demonstrating that the model accurately represents controller behavior and parameterization and is suitable for RMS-based stability analyses and grid compliance studies. Beyond the validation of a specific implementation, the study establishes a structured methodology for benchmarking PPC models against physical hardware using CHiL testing. Although the presented case focuses on a PPC deployed in a PV plant, the proposed validation framework is generally applicable to other IBR technologies operating under PPC supervision. The adopted RMS modeling approach is appropriate for plant-level supervisory control dynamics. However, EMT-level inverter behavior and unbalanced conditions remain outside the scope of this work and represent a direction for future research.

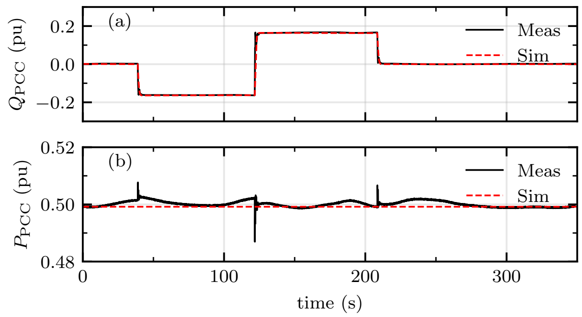

Fig. 5. Results of Power factor Control test (a) Positive sequence reactive power, (b) Positive sequence active power.

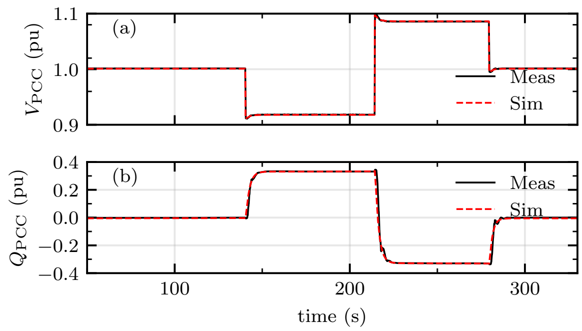

Fig. 6. $Q(V)$ Control test: (a) Positive sequence voltage, (b) Positive sequence reactive power.

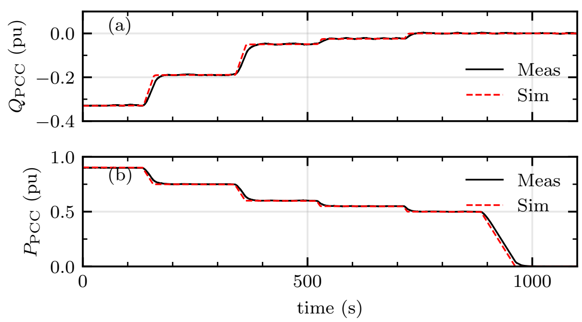

Fig. 7. $Q(P)$ Control test: (a) Positive sequence reactive power, (b) Positive sequence active power.

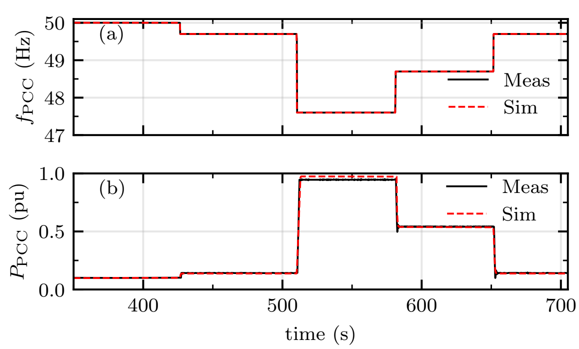

Fig. 8. LFSM Control test: (a) Frequency, (b) Positive sequence active power.

REFERENCES

[1] D. Audring and A. Kuri, "Modelling and challenges of integration of large renewable power plants," in *2021 56th International Universities Power Engineering Conference*. IEEE, 2021, pp. 1–6.

[2] S. Kamalhosseini, I. Burlakin, A. Kuri, G. Mehlmann, and M. Luther, "Grid-forming capability of power plant control: optimization through battery energy storage integration," *IET Conference Proceedings*, vol. 2024, no. 16, pp. 953–960, 2025.

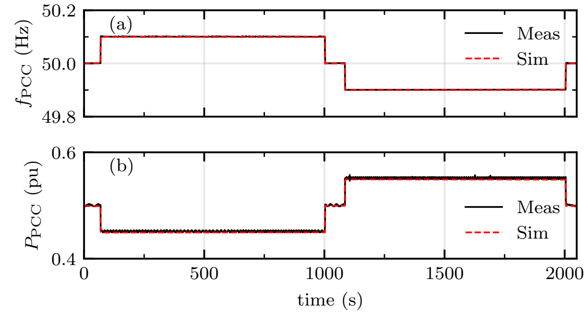

Fig. 9. FSM Control test: (a) Frequency, (b) Positive sequence active power.

[3] "IEEE standard for interconnection and interoperability of inverter-based resources (ibrs) interconnecting with associated transmission electric power systems," *IEEE Std 2800-2022*, 2022.

[4] A. Kuri and E. Brackenhammern, "Challenges for integration of renewable energy in public grid," in *21st Wind & Solar Integration Workshop*, 2022, pp. 599–606.

[5] T. Ernst and K. Sletten, "Commission testing methods for protection systems," in *2017 70th Annual Conference for Protective Relay Engineers*, 2017, pp. 1–9.

[6] A. Etxegarai, P. Eguia, E. Torres, G. Buigues, and A. Iturregi, "Current procedures and practices on grid code compliance verification of renewable power generation," *Renewable and Sustainable Energy Reviews*, vol. 71, pp. 191–202, 2017.

[7] S. Sommerville, G. A. Taylor, and M. Abbod, "Development and deployment of generic models for grid code compliance studies," in *2024 IEEE PES Innovative Smart Grid Technologies Europe*. IEEE, 2024, pp. 1–5.

[8] Y. Mitsugi, T. Terazono, and H. Hashiguchi, "Comparison of field test and controller hardware-in-the-loop simulation results of utility-scale battery energy storage system," in *2024 IEEE PES Innovative Smart Grid Technologies Europe*. IEEE, 2024, pp. 1–5.

[9] M. Farraj, R. Salehi, A. Momeni, A. Zamani, and R. Kadem, "Validation of the power plant controller for frequency support applications using hardware-in-the-loop testing," in *2022 IEEE Electrical Energy Storage Application and Technologies Conference*. IEEE, 2022, pp. 1–5.

[10] R. K. R. Kumar, S. Soni, D. Anichkov, and N. Milam, "Hardware-in-the-loop validation of utility-scale power plant controllers for inverter-based resources," in *2025 IEEE PES Grid Edge Technologies Conference & Exposition (Grid Edge)*. IEEE, 2025, pp. 1–5.

[11] A. Bammes *et al.*, "De-risking grid forming battery energy storage projects - grid code compliance testing of a 50 mw storage system using control-hardware-in-the-loop," in *CIGRE 2025 International Symposium, Montreal*. in press, 2025, pp. 1–9.

[12] VDE-AR-N-4110, "Technical requirements for the connection and operation of customer installations to the medium voltage network (tcr medium voltage) english translation of vde-ar-n 4110:2018-11."

[13] VDE-AR-N-4120, "Technical requirements for the connection and operation of customer installations to the high voltage network (tcr high voltage)-english translation of vde-ar-n 4120:2018-11."

[14] VDE-AR-N-4130, "Technical requirements for the connection and operation of customer installations to the extra high voltage network (tcr extra high voltage) english translation of vde-ar-n 4130:2018-11."

[15] A. Yazdani and R. Iravani, *Voltage-sourced converters in power systems: Modeling, control, and applications*. Hoboken, NJ and Piscataway, NJ: Wiley and IEEE Press, 2010.

[16] ENTSO-E, "Limited frequency sensitive mode: Entso-e guidance document for national implementation for network codes on grid connection."

[17] ENTSO-E, "Frequency sensitive mode: Entso-e guidance document for national implementation for network codes on grid connection."

[18] FGW (Fördergesellschaft Windenergie und andere Dezentrale Energien), "Technical guidelines for power generating units and systems, part 3 (tg3): Determination of the electrical characteristics of power generating units and systems, storage systems as well for their components in medium-, high- and extra-high voltage grids," 2018.

[19] FGW, "Technical guidelines for power generating units and systems, part 4 (tg4): Requirements for modelling and validation of simulation models of electrical properties of generation units and plants, storage systems and theirs components," 2022.